

## Flume observations of enhanced fine-particle deposition to permeable sediment beds

J. Stephen Fries<sup>1</sup> and John H. Trowbridge

Applied Ocean Physics and Engineering Department, Woods Hole Oceanographic Institution, 89 Water Street, Woods Hole, Massachusetts 02543

### Abstract

Predictions of the deposition rate of fine particles are integral to the study of the transport of many constituents, including contaminants and organic matter. Generally, fine-particle deposition rates are assumed to be equivalent to the suspension settling velocity. Deposition rates in excess of settling are considered enhanced. Flume observations of deposition were made using treatments that covered a wide range of flow, particle, and bed conditions. No enhancement was observed to impermeable boundaries. Specific treatments of sand bed experiments demonstrated large enhancements (up to eight times settling). For coarser sediment beds, little to no enhancement was observed. Previously identified mechanisms that could alter deposition rates, such as topography and aggregation, were dismissed using careful flow and particle size distribution measurements. Correlations between drag coefficient and deposition suggest that the mechanisms delivering additional particles to the sediment also reduce the effective drag of the bed on the flow. This is consistent with velocity slip at the sediment–water interface. Another trend evident in the data is a dependence on the ratio of the bed grain size to particle diameter. Small ratios were associated with large enhancements, consistent with the idea that filtration within the sediment could be retaining delivered particles. In concert, fluid incursions and bed filtration might be capable of increasing the particle flux to the bed. The observation of enhanced deposition to flat sediment beds reinforces the importance of permeable sediments to the transport of particles from the water column to the sediment bed.

Dispersal of fine particles depends critically on the deposition rate (e.g., Nittrouer and Wright 1994). Accurate predictions of deposition are important to the calculation of sediment budgets and offshore transport of sediment from rivers or coastal marshes (e.g., Wheatcroft et al. 1996). The most common assumption in fine-particle deposition is that particles simply settle under gravity (Einstein 1968). It is possible that other mechanisms could mediate the flux of fine particles to permeable sediment beds, including delivery of particles by near-bed turbulence (Dade et al. 1991), interfacial flows near bed topography (Huettel et al. 1996), alteration of interfacial flows by bed load (Packman and Brooks 2001), and filtration at the sediment–water interface (Hoyal et al. 1997).

It is helpful to define particle deposition as two steps: delivery and retention. These steps are sequential, and a coupling of the two is required to result in particle deposition.

---

<sup>1</sup> To whom correspondence should be addressed. Present address: Institute of Marine and Coastal Sciences, Rutgers University, 71 Dudley Road, New Brunswick, New Jersey 08901 (fries@imcs.rutgers.edu).

### Acknowledgments

Throughout the research described in this study, valuable advice and guidance was received from Ole Madsen, Robert Wheatcroft, and Wade McGillis. The authors thank the Reinhart Coastal Research Center at the Woods Hole Oceanographic Institution for use of the flume facilities. Jay Sisson provided essential assistance during experimentation, and Rob Olsen provided access to a Coulter counter. Gary Taghon participated in many helpful discussions of this manuscript. Two anonymous reviewers provided many helpful and insightful comments to improve this manuscript. Graduate student support for J.S.F. (at WHOI) was provided by an NSF Coastal Fellowship and by the Cooperative Institute for Climate and Ocean Research (NOAA). This is contribution 10674 from Woods Hole Oceanographic Institution.

Identification of the controls for both delivery and retention of fine particles would improve models of fine-particle deposition. Einstein (1968) conducted a flume study of fine-particle deposition to gravel beds and measured particle deposition rates that were approximately the same as the settling velocity of the suspension. The author concluded that no additional particles were being delivered to the gravel by the energetic turbulent flows near the bed. An alternative explanation for these results is that large amounts of particles were delivered to the bed, but very little of this material was retained. Therefore, gravity provided the only net flux of particles. Increased particle delivery due to increases in boundary roughness was integral to a deposition model proposed by Dade et al. (1991). Retention via filtration of delivered particles from the flow by sand grains at the interface (Hoyal et al. 1997) would lead to enhancement. In this study, the particles were deposited to sediment beds of distinctly coarser grains; that is, the sediment bed was not a source of additional material to the water column.

For flat sediment beds, the particle motion near the bed depends on the fluid flow structure within the viscous sublayer. The structure is defined by upward “bursts” and downward “sweeps” near the bed (e.g., Grass 1971). Particles respond readily to bursts that entrain them from the bed, whereas particles appear to simply settle through the sublayer, without noticeable increases in deposition due to sweeps (Nino and Garcia 1996). The entrainment of particles is hindered when the particles are significantly smaller than the bed grains. This “hiding” effect prevents entrainment under flow conditions capable of entraining the same particles on a smooth boundary (Nino and Garcia 1996). The flows within the viscous sublayer might play a role in controlling the fine-particle flux at the sediment–water interface.

This paper describes an investigation of fine-particle deposition to flat sediment beds. First, the large set of variables

pertinent to fine-particle deposition is reduced to a set of important parameters. Second, flume experiments designed to cover a wide and oceanographically relevant range of these parameters are described. Third, results are presented, including the contrast of solid and permeable boundaries with regard to flow conditions and deposition results. Discussion of these results includes comparison to the limited results previously published in other studies and the steps taken to ensure that other mechanisms, principally aggregation and topography, did not play a role in these observations. Fourth, evidence supporting the mediation of deposition by diffusion across and filtration at the sediment-water interface is presented.

### Important parameters

The design of experiments to reveal the mechanisms responsible for mediating fine-particle deposition requires recognition of the important parameters describing deposition. These parameters will be used to describe the net flux of particles to the bed ( $F$ ) defined as the product of the suspension concentration ( $\bar{C}$ ) and deposition velocity ( $w_d$ ) (Eq. 1).

$$F = \bar{C}w_d \quad (1)$$

Deposition velocities in excess of the settling velocity ( $w_s$ ) are considered enhanced; therefore, the most appropriate parameter for describing the deposition is the enhancement factor (Eq. 2).

$$E_d = \frac{F}{\bar{C}w_s} = \frac{w_d}{w_s} \quad (2)$$

Values of  $E_d$  greater than unity indicate conditions where enhanced deposition occurs. The remaining parameters relevant to fine-particle deposition can be grouped into three categories: those characterizing the flow, those characterizing the bed, and those characterizing the particle suspension.

Studies of boundary layer flows in open channels (e.g., Nezu and Rodi 1986) have identified the critical variables describing the structure of the flow: fluid density ( $\rho$ ), fluid viscosity ( $\nu$ ), channel depth ( $h$ ), boundary roughness ( $k_s$ ), and mean channel velocity ( $U$ ). The flow exerts a boundary shear stress ( $\tau_b$ ) on the channel bottom that can also be described as a shear velocity (Eq. 3).

$$u_* = \sqrt{\tau_b/\rho} \quad (3)$$

Measurements of boundary layer flow are often summarized in terms of a drag coefficient (Eq. 4).

$$C_D = \left(\frac{u_*}{U}\right)^2 \quad (4)$$

Two dimensionless parameters are needed to describe the attributes of the flow (Eq. 5 and 6).

$$R_* = \frac{u_*k_s}{\nu} \quad (5)$$

$$R_h = \frac{Uh}{\nu} \quad (6)$$

The grain Reynolds number ( $R_*$ ) describes the nature of the

near-bed flows, whereas the channel Reynolds number ( $R_h$ ) describes the turbulent nature of the entire boundary layer. This set of parameters becomes an expression for describing the channel drag coefficient in terms of the open channel boundary layer flow characteristics (Eq. 7).

$$C_D = f(R_*, R_h) \quad (7)$$

For permeable boundaries, properties of the sediment affect the flow at the sediment-water interface. The sediment bed is characterized by the bed grain size ( $d_g$ ), permeability ( $K$ ), and porosity ( $\phi$ ). All three sedimentary variables can be related using the Carman-Kozeny equation (Eq. 8; Kozeny 1927; see Boudreau 1997).

$$K = \frac{\phi^3}{180(1-\phi)^2} d_g^2 \quad (8)$$

For flat sediment beds, the boundary roughness ( $k_s$ ) and bed grain size are the same quantity; therefore, only one additional parameter is needed (Eq. 9).

$$R_K = \frac{u_*\sqrt{K}}{\nu} \quad (9)$$

The bed Reynolds number ( $R_K$ ) has been recognized in the porous media literature as important to describing the dominant drag mechanisms for interstitial flow (Ward 1964). The flow expression now includes four parameters (Eq. 10).

$$C_D = f(R_*, R_h, R_K) \quad (10)$$

Variables describing particle suspension play an important part in the description of deposition. In addition to the concentration and settling velocity presented earlier, the particle diameter ( $d_p$ ), density ( $\rho_p$ ), and diffusivity ( $D$ ) describe the suspension completely. A potential list of dimensionless parameters is shown in Eqs. 11–15.

$$\rho' = \frac{\bar{C}}{\rho} \quad (11)$$

$$R = \frac{w_s}{u_*} \quad (12)$$

$$t_p = \frac{\rho_p}{18\rho} \left(\frac{u_*d_p}{\nu}\right)^2 \quad (13)$$

$$Sc = \frac{\nu}{D} \quad (14)$$

$$D_R = \frac{d_g}{d_p} \quad (15)$$

Some of these parameters have negligible influences on fine-particle deposition in water. Unlike particles in air, the difference in density between particles and water is small, limiting the anomaly in the fluid density due to particle concentration ( $\rho'$ ) and the importance of particle inertia indicated by the particle relaxation time ( $t_p$ ). Another implication of limited particle inertia is the ability to neglect the Rouse parameter ( $R$ ) because of the dominance of the turbulent fluid motions over the gravitational settling of particles. Note that the elimination of  $R$  from consideration is primarily related to the instantaneous motion and distribution

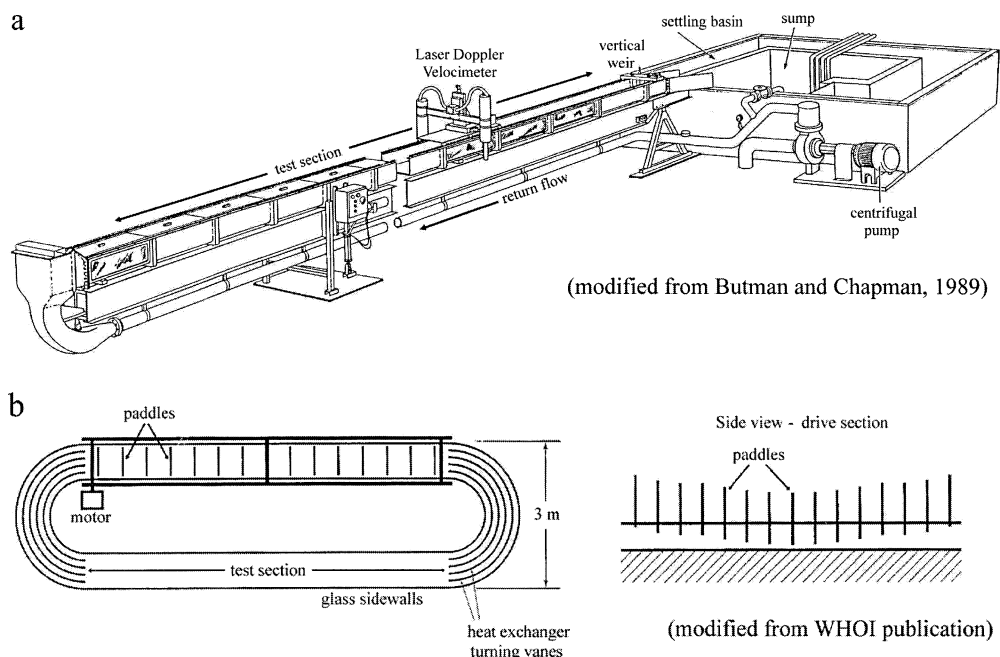


Fig. 1. Diagrams of flume facilities. (a) 17M. Sediment beds installed in final 11 m of raceway. (b) RTF. Sediment beds occupied entire test section. Flow sampling located 6 m from start of sediment in both flumes.

of particles in the water column. This argument does not preclude the settling velocity from describing the overall particle flux to the boundary. Particle diffusivity based on Brownian motion (Einstein 1906) is typically of the order  $10^{-9} \text{ cm}^2 \text{ s}^{-1}$  for fine particles in water, much smaller than the viscosity of the fluid itself (on the order of  $10^{-2} \text{ cm}^2 \text{ s}^{-1}$ ). A large Schmidt number ( $Sc$ ) indicates the absence of significant particle diffusion. This leaves only one parameter, the grain diameter ratio ( $D_R$ ), to add to the list of relevant parameters. The relative size of the particles to the bed grains describes the ability of the suspension to enter and move within the sediment and is a critical parameter in expressions of the filtration efficiency of a sediment bed (see review by McDowell-Boyer et al. 1986). This ratio also is important in the suppression of entrainment of delivered particles at the sediment–water interface (Nino and Garcia 1996).

Choosing three of the parameters describing flow and focusing on the measurements of flux, the final dimensionless expression becomes Eq. 16.

$$E_d = f(C_D, R_*, R_K, D_R) \quad (16)$$

Of these parameters, three ( $R_*$ ,  $R_K$ , and  $D_R$ ) will be varied in experiments designed to explore a wide and realistic range of these parameters. The other two ( $E_d$  and  $C_D$ ) will be measured. This study will reveal the relationships between these parameters and the basis for an understanding of the mechanisms that enhance fine-particle deposition.

## Methods

*Flume facilities*—Observations were made in two flumes: the “17-Meter Flume” (17M) described by Butman and

Chapman (1989) and the “Racetrack Flume” (RTF), both located in the Reinhart Coastal Research Laboratory at the Woods Hole Oceanographic Institution (Fig. 1). The essential difference between these flumes is the method used to recirculate the water. In the 17M, flow passes through the channel (17.3 m long, 60 cm wide, 30 cm deep) and into a sump that drains into a centrifugal pump. Note that the settling basin was bypassed for these experiments. Water depth in the channel is adjustable via a downstream weir. The RTF, a design based on the flume described by Nowell et al. (1981), is an oval design with a linear paddle drive designed to maintain vertical paddle orientation while in the flow. The test section (7.5 m long, 75 cm wide, 30 cm deep) is positioned on the opposite side from the paddles. All flume experiments used  $10\text{-}\mu\text{m}$  filtered seawater.

Both flumes exhibit minimal cross-channel flow structure over the range of flows used in this study. Extensive calibration of the 17M by Trowbridge et al. (1989) revealed that the alongstream flow varies by  $<25\%$  over the middle 70% of the channel, whereas the shear velocity remains within 10% of the centerline value in this same region. The RTF is more susceptible to cross-channel flows because of its oval design. Flow measurements reveal 20% reduction in shear and mean alongstream velocities across 66% of the channel width (unpubl. data). Both flow statistics drop off another 10% within 10 cm of the walls. In both flumes, little change in deposition results were expected because of cross-stream flow variability.

Velocity measurements were made with a laser Doppler velocimeter (Agrawal and Belting 1988). Experimental flow data were fit to an expression for open channel, turbulent boundary layers (Eq. 17).

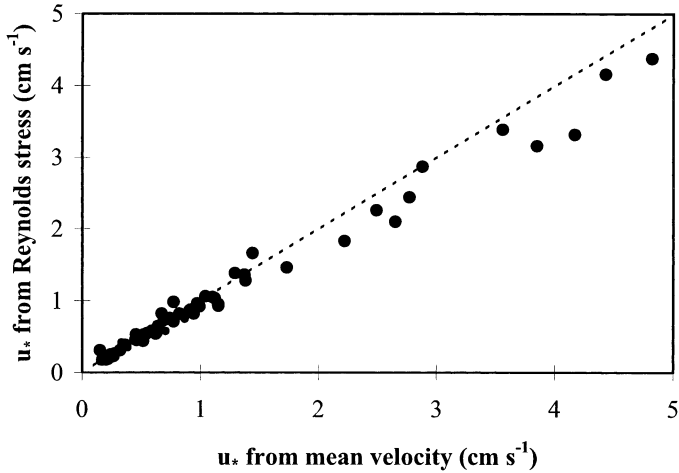


Fig. 2. Comparison of shear velocities from profiles of mean velocity and Reynolds stress. Both sediment and impermeable bed experiments from both flume facilities are included. Dashed line represents 1:1 correlation.

$$u(z) = \frac{u_*}{\kappa} \ln\left(\frac{z + \Delta}{d_g}\right) + B(R_*)u_* + W(z) \quad (17)$$

$z$  is the elevation above the boundary,  $\kappa$  is the von Karman constant (0.4),  $B$  is a function of the grain Reynolds number (see fig. 20.21, p. 583, in Schlichting 1968),  $\Delta$  is the displacement of the profile, and  $W$  is the profile due to the wake layer (Eq. 18).

$$W(z) = \frac{2\Pi}{\kappa} u_* \sin^2\left(\frac{\pi z + \Delta}{2h}\right) \quad (18)$$

$\Pi$  is a parameter that typically ranges from 0 to 0.4 (Coles 1956). Three fit parameters were used ( $u_*$ ,  $\Delta$ , and  $\Pi$ ). All reported values of shear velocity in this study were obtained from these fits.

Profiles of Reynolds stress provided confirmation of the shear velocity estimates from velocity profiles. In open-channel turbulent boundary layer flows, the ideal profile of Reynolds stress is approximately linear approaching the boundary in Eq. 19.

$$\overline{u'w'}(z) \cong u_*^2 \left(1 - \frac{z}{h}\right) \quad (19)$$

This profile does not extend all the way to the bed because of the restriction of vertical velocity fluctuations at a solid boundary. Shear velocities from fits to Reynolds stress profiles compare well with estimates from mean velocity profiles (Fig. 2). The deviation from a 1:1 correlation for high  $u_*$  treatments could be due to the greater influence of the wake layer on the mean velocity relative to the Reynolds stress profile at higher flows.

Flume experiments included both permeable and impermeable boundaries. Flat sediment beds were laid over the channel bottom to a depth of 2–4 cm and a length of 11 and 6.6 m in the 17M and RTF, respectively. Marble beds were three layers deep and 5 m long in both flumes. Upstream of the sediment, panels were installed level with the sediment

Table 1. Treatments used in flume experiments.

Bed	No. of runs	$u_*$ (cm s <sup>-1</sup> )	$h$ (cm)	$d_g$	$K$ (cm <sup>2</sup> )
PVC	20	0.10–1.38	11.8–13.5	—	—
Sand	16	0.34–1.49	13.0–13.2	350 $\mu$ m	$2.5 \times 10^{-7}$
Sand	4	0.34–0.80	12.3–13.0	400 $\mu$ m	$2.7 \times 10^{-7}$
Coarse sand	12	0.23–1.05	11.8–12.5	550 $\mu$ m	$3.0 \times 10^{-7}$
Gravel	3	0.43–1.25	12.0–12.2	1.3 mm	$2.8 \times 10^{-6}$
Marbles	17	0.20–4.19	12.3–12.8	1.23 cm	$1.4 \times 10^{-3}$

surface. Table 1 details the various sediments used for these experiments. Permeability values were determined using falling- or constant-head permeability tests as described by Al-Khafaji and Andersland (1992). Bottom topography was eliminated and flat-bed conditions were verified by visual inspection from above and through sidewall windows. For smooth-bed experiments in the 17M, a false bottom with three  $8 \times 20 \times 0.4$ -cm-deep indentations was installed. Indentations were filled, flush with the bottom, with one of two classes of glass beads to serve as particle traps. The nominal size ranges for the glass beads (Cataphote) were 250–350  $\mu$ m and 420–590  $\mu$ m. No particle traps were installed in the RTF.

The particle suspensions for flume experiments were chosen to cover a wide range of settling velocities. Four suspensions were used in this study (Table 2). MoSci Corporation supplied three classes of solid glass beads. Particles with nearly neutral density (Sontek) were used as the fourth suspension. Grain size distributions provided by the manufacturers were verified in the laboratory by conducting particle size analysis using a Coulter counter model II. Samples were analyzed using a 100- $\mu$ m orifice that resolves diameters from 1 to 64  $\mu$ m.

*Deposition measurements*—The procedure for introducing particle suspensions to the flumes was designed to provide a well-mixed initial condition. Fine particles were added after the flow stabilized. Suspensions were mixed with flume water and introduced to the flume sump (17M) or in the turns downstream of the test section over a flume transit time (RTF). Particles were allowed at least two additional transit times through the system prior to sampling to allow particles to mix into the system. Initial suspension concentrations of 4–40 mg L<sup>-1</sup> were used.

Water samples were collected during flume experiments to monitor the amount of fine particles in suspension over time. Water samples (1 liter) were taken at regular intervals

Table 2. Suspensions used for flume experiments.

Suspension	Material	Density (g cm <sup>-3</sup> )	$d_p$ range ( $\mu$ m)	Median $d_p$ ( $\mu$ m)	$w_s$ (cm s <sup>-1</sup> )
I	Solid glass	2.5	5–25	12	0.010
II	Solid glass	2.5	3–25	8	0.007
III	Solid glass	2.5	20–60	30	0.030
IV	Hollow glass	1.4	10–30	13.5	0.004

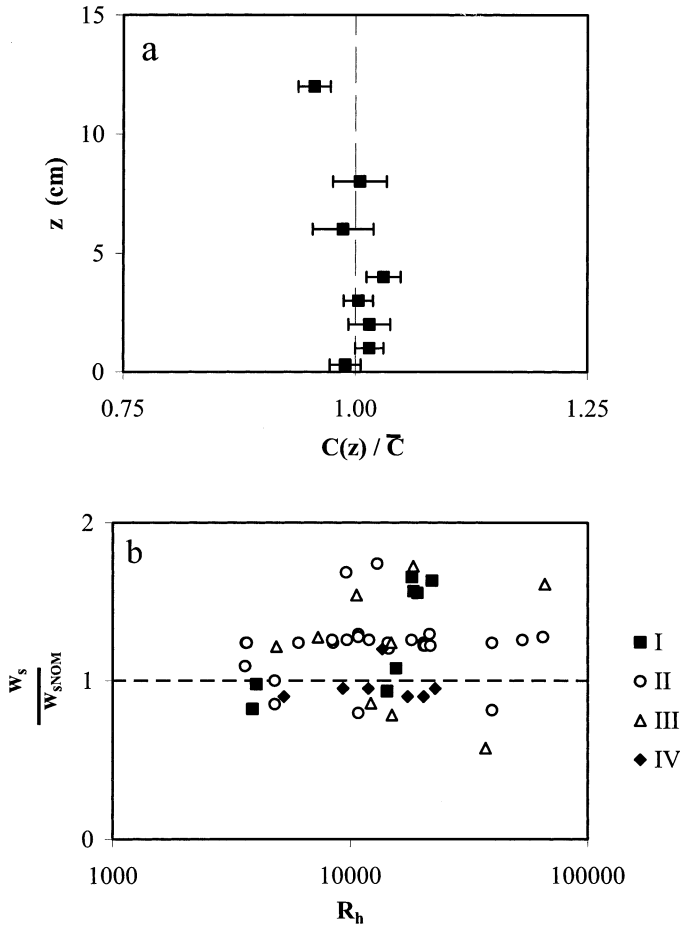


Fig. 3. Experimental confirmation of fine-particle suspension characteristics. (a) Fine-particle concentration profile. Concentration profile normalized by the depth-averaged concentration. Error bars represent  $\pm 1$  SE. (b) Particle settling velocities from initial water samples ( $t = 0$ ) relative to channel Reynolds number. Settling velocities normalized by the nominal (NOM) settling velocity from the source material. The horizontal line represents a ratio of 1. Points grouped with respect to the suspension number (I–IV).

of 20–30 min for the duration of the 3-h experiments for all suspensions except III. Experiments for this suspension were shortened to 30 min with 3–5-min sampling intervals because of the larger settling velocity. For most experiments, water samples were collected at both ends of the test section. A single siphon tube was used at the upstream end (“head”) of the channel. At the downstream end (“tail”), a siphon with multiple ports was installed on the flume centerline. In most cases, all ports were combined to obtain a single sample. Observations of the concentration profile in the flume confirmed that the water column was well mixed (Fig. 3a) as expected for slow-settling particles. Ambient material appeared to have a negligible settling velocity in experiments without fine-particle additions (Fries 2002); therefore, ambient concentration was assumed to be constant for the duration of any flume run.

Water samples were poured through a 45- $\mu\text{m}$  sieve onto a weighed 1.2- $\mu\text{m}$  membrane for vacuum filtration (Osmonics MCE Membranes). The sieve was not used for experi-

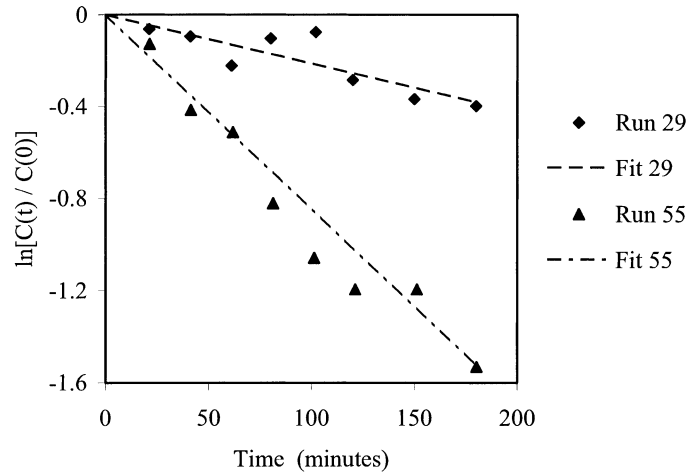


Fig. 4. Examples of time series data from water samples. Dashed lines are linear fits for both data sets. Experiments chosen represent the range of concentration decay observed.

ments with the largest suspension (III) to avoid selective removal of the coarsest fraction. Each filter membrane was weighed to determine the total amount of material in the sample. A detection limit of 0.2 mg L<sup>-1</sup> was determined for this method.

The total mass measurements were fit to an equation describing the loss of suspended particles to the boundary as an exponential decay (Eq. 20).

$$\bar{C}(x, t) = \bar{C}_0 \exp\{-\alpha(x)[t - t_0(x)]\} + \bar{C}_a \quad (20)$$

$$\bar{C}_0 = \frac{m_{\text{add}}}{V_f} \quad (21)$$

$x$  is the downstream coordinate,  $t$  is the time elapsed,  $\alpha$  is the decay rate for the suspension,  $t_0$  is the time lag due to initial mixing in the flume,  $m_{\text{add}}$  is the mass of particles added,  $V_f$  is the total volume of the flume,  $\bar{C}_a$  is the ambient concentration (from control samples), and overbars represent depth-averaged values. The use of an exponential decay is based on the definition of flux (Eq. 1) and is consistent with similar work for solute efflux from sediment (e.g., Richardson and Parr 1988). The fit to the decay equation involves adjusting the values for  $t_0$  and  $\alpha$ . Curve fits were made to both the head ( $x = 0$ ) and tail ( $x = L$ , the length of the sediment bed) time series data using a least squares method. Decay rates from both the head and tail were found to be essentially equal for all experiments; therefore,  $\alpha$  is assumed to be independent of  $x$ . Examples of curve fits to time series data are presented in Fig. 4.

Measurements of concentration were converted to deposition velocities through the comparison of samples from the head and tail of the test section. Consider the rate of change of concentration in the test section from the decay expression in Eq. 22.

$$\frac{\partial \bar{C}}{\partial t} = \bar{C}(x, t) \left[ -\alpha \left( 1 + U \frac{\partial t_0}{\partial x} \right) \right] \quad (22)$$

The loss of mass from the water column can also be estimated from the flux definition as in Eq. 23.

$$\frac{\partial \bar{C}}{\partial t} = \bar{C}(x, t) \left[ \frac{-w_d}{h} \right] \quad (23)$$

Equating these expressions leads to an expression for the deposition velocity as a function of the fit parameters from the head and tail time series data (Eq. 24).

$$w_d = h\alpha \left( 1 + U \frac{\partial t_0}{\partial x} \right) = h\alpha \left( 1 + U \frac{t_0(L) - t_0(0)}{L} \right) \quad (24)$$

Note that the assumption of a linear trend in  $t_0$  with  $x$  is based on the definition of a constant deposition velocity in the test section and is consistent with the idea that  $t_0$  represents a lag time correction in the profile fits. A similar calculation of the change from the tail to the head reveals the amount of particles lost to the rest of the flume. For both flumes, all the loss estimates were smaller than the settling velocity (Fries 2002) and, consequently, considered negligible.

The distribution of particle sizes in the suspension determines the appropriate settling velocity for comparison to deposition measurements. Coulter counter analysis provided a definite measure of the particle size population at the start of all experiments. Small water samples (50 ml) were collected directly from the flume along with samples for total mass analysis. The median particle size ( $d_{p50}$ ) was calculated for each sample based on the condition

$$\int_{d_{\min}}^{d_{p50(t)}} n(\sigma, t) d\sigma = \frac{1}{2} \quad (25)$$

where the subscript “min” refers to the minimum diameter in the count,  $\sigma$  is an integration variable, and  $n$  is the particle count. The settling velocity of the median particle diameter was compared to that measured for the source material (Fig. 3b). For all the suspensions, scatter was evident, suggesting that the alteration of the suspension might be due to loss of dry particles during handling, not to a systematic bias in the experiments. The settling velocity measured for water samples was used in the calculation of  $E_d$  for most experiments. In those experiments without this measurement available, the average of all other measurements for that suspension was used (Table 4).

*Sediment core analysis*—To verify that particles lost from suspension were deposited to the bed, cores were taken from the sand bed during experiments. At least seven cores were collected prior to (“pre”) and following (“post”) each flume run. Cores were collected with cut 5 cc syringes (1.4 cm diameter) within 20 cm of the flume centerline at a minimum of three downstream positions, all further than 1.5 m from the start of the sediment bed. The deposited mass was measured by diluting each core with distilled water then passing the sample through a 45- $\mu\text{m}$  sieve. As in the case for water samples, the sieve was not used for samples from experiments with suspension III to avoid unintended removal of particles. The fluid recovered after repeating this procedure three times was vacuum filtered through a 1.2- $\mu\text{m}$  membrane. The rinsed sediment was dried and weighed to estimate the total mass of the core. For smooth-bed runs, each particle trap was treated as a core and siphoned directly into

a bottle. One “pre” core and two “post” cores were collected for each run, and samples were handled using the procedure described for water samples.

Calculation of the mass deposited per core ( $m_c$ ) was the difference between preflume and postflume cores, adjusted by the core weights

$$m_c = m_{\text{post}} - m_{\text{pre}} \frac{M_{\text{post}}}{M_{\text{pre}}} \quad (26)$$

where  $m$  is the mass of particles in the core,  $M$  is the total mass of the core, and the subscripts “pre” and “post” denote the time of core collection. The total mass deposited can be calculated from the start and end of the concentration time series

$$m_{\text{loss}} = V_f [\bar{C}(0) - \bar{C}(t_{\text{core}})] \quad (27)$$

where  $t_{\text{core}}$  is the time elapsed between the start of the run and collection of “post” cores. If the mass of particles is evenly spread over the test section, then the ratio of the area of the core ( $A_c$ ) to the entire sediment bed can be used to predict the amount of fine particles in a core

$$m_w = \frac{A_c}{b_f L} m_{\text{loss}} = \frac{A_c}{b_f L} V_f [\bar{C}(0) - \bar{C}(t_{\text{core}})] \quad (28)$$

where  $b_f$  is the flume width. Additional cores (up to 90) collected during a few experiments did not indicate that selected sampling locations produced any bias in the measurement of mass in cores (Fries 2002).

For one treatment (400- $\mu\text{m}$  sand and suspension IV), cores from three experiments were sectioned to determine the vertical distribution of deposited particles in the sediment. Four sections were isolated: 0–2 mm, 2–5 mm, 5–10 mm, and >10 mm. Most cores were >30 mm in length. Mass determination for each section was done in the same manner as the whole-core method.

A control experiment was conducted to ensure that the coring and sectioning procedures did not significantly alter the concentration profile within the sediment bed. A suspension of 100 mg  $\text{L}^{-1}$  was allowed to settle under still water conditions to a sand bed. Cores were collected 1 and 3 h after addition. Under still water, all deposited particles should be in the top sediment section (0–2 mm). Particles deeper in the bed were assumed to have moved during the coring procedure.

## Results

*Deposition measurements*—Impermeable boundaries were used as a control for deposition measurements. Results from water samples collected during flume experiments over polyvinyl chloride (PVC) beds confirmed that the deposition velocity was approximately the same as settling for all suspensions over the range of flows possible in the flume facilities (Fig. 5a). This result confirmed that the flumes could be used to measure deposition rates as small as the settling velocity for the test suspensions. The total amount of deposition was qualitatively confirmed by the smooth bed particle trap results (Fig. 5b). The traps reproduce the relative magnitudes of the total losses from the water column;

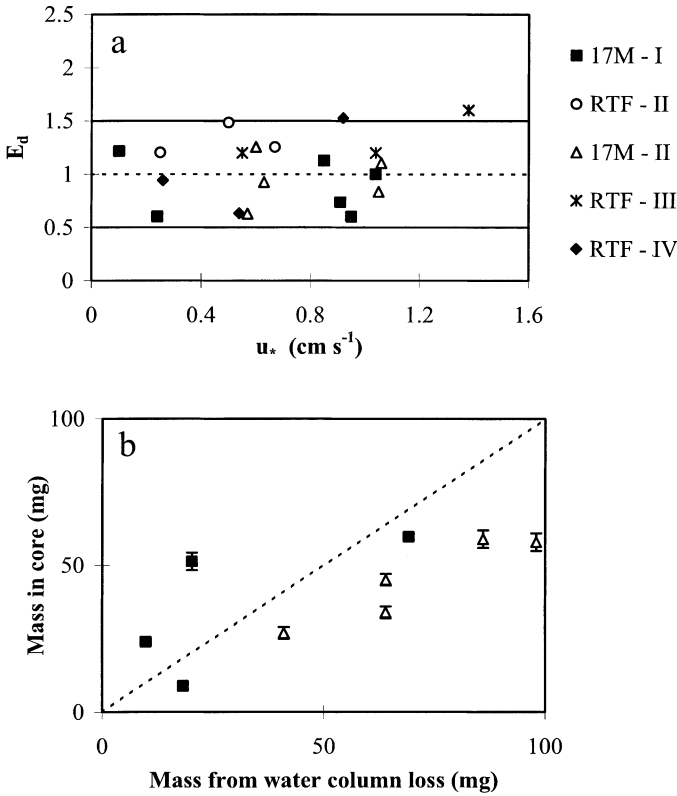


Fig. 5. Deposition results for all PVC experiments. (a) Deposition based on loss from water column. Horizontal lines denote the adopted range of values for no enhancement ( $E_d = 1 \pm 0.5$ ). Errors (bars omitted for clarity) were typically  $\pm 0.5 E_d$  units. (b) Smooth-bed particle trap results for PVC experiments in 17M. Dashed line represents 1:1 relationship. Error bars represent  $\pm 1$  SD. Points grouped by flume (17M or RTF) and suspension number (I-IV).

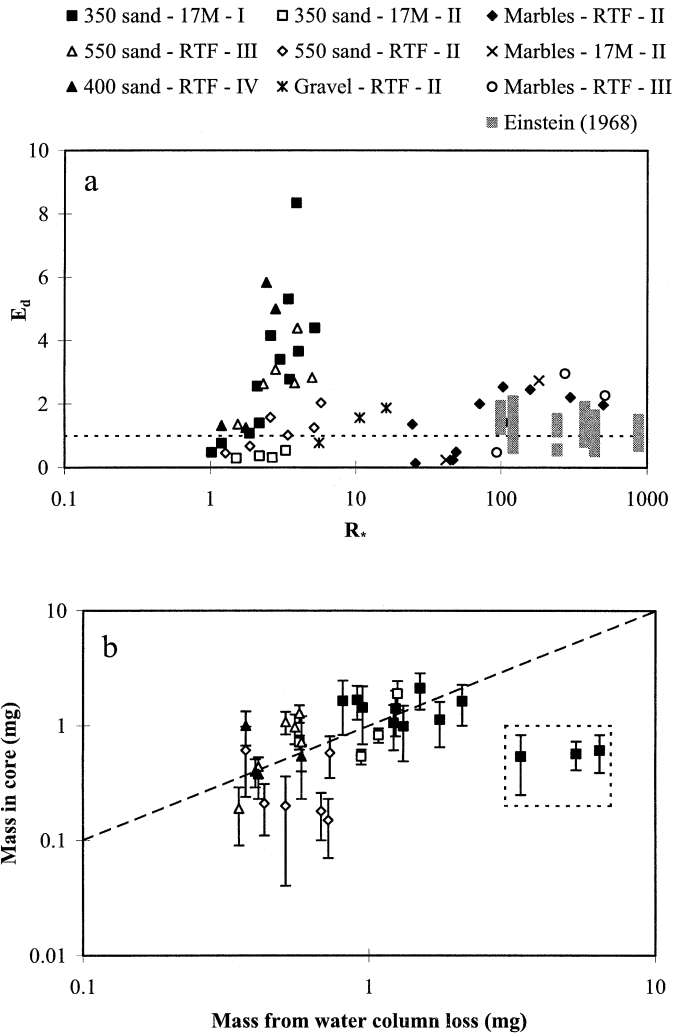


Fig. 6. Deposition results for sediment bed experiments. (a) Deposition based on loss from water column. Dashed horizontal line denotes the value for no enhancement ( $E_d = 1$ ). Errors (bars omitted for clarity) were typically  $\pm 0.5 E_d$  units. Results from Einstein (1968) included for reference. (b) Sediment bed core results for all sand experiments. Dashed line represents 1:1 relationship. Error bars represent  $\pm 1$  SD. Points grouped by sediment type (350-, 400-, and 550- $\mu\text{m}$  sands; 1.3-mm gravel; 1.2-cm marbles), flume (17M or RTF), and suspension number (I-IV).

Table 3. Data from PVC deposition experiments.

Flume	$u_*$ ( $\text{cm s}^{-1}$ )	Suspension	$w_s$ ( $\text{cm s}^{-1}$ )	$w_d$ ( $\text{cm s}^{-1}$ )	$C_D$ ( $\times 10^4$ )	$m_c$ (mg)
17M	0.24	I	0.0088	0.0053	36	9
17M	0.10	I	0.0074	0.0090	43	—
17M	1.04	I	0.0147	0.0147	38	—
17M	0.95	I	0.0140	0.0084	37	60
17M	0.85	I	0.0149	0.0168	39	51
17M	0.91	I	0.0141	0.0104	41	24
RTF	0.50	II	0.0091	0.0135	40	—
RTF	0.25	II	0.0054	0.0065	48	—
RTF	0.67	II	0.0094	0.0118	35	—
17M	0.60	II	0.0043	0.0054	41	58
17M	0.57	II	0.0070	0.0044	38	59
17M	0.63	II	0.0069	0.0064	48	27
17M	1.05	II	0.0067	0.0056	38	34
17M	1.06	II	0.0066	0.0073	37	45
RTF	1.04	III	0.0150	0.0180	24	—
RTF	0.55	III	0.0150	0.0180	27	—
RTF	1.38	III	0.0150	0.0240	22	—
RTF	0.54	IV	0.0038	0.0024	28	—
RTF	0.92	IV	0.0038	0.0058	24	—
RTF	0.26	IV	0.0036	0.0034	21	—

however, there is a decline for the highest concentration runs. All data from impermeable bed experiments are listed in Table 3.

The results from deposition experiments with sediment beds can be divided into two sets. First, for large-grain Reynolds numbers, little to no enhancement was observed (right side of Fig. 6a). This observation is consistent with the results from Einstein (1968) for very rough beds. Second, finer sediment treatments revealed a set of conditions that led to enhancement (left side of Fig. 6a). Three specific treatments demonstrated large enhancements: suspension I and 350- $\mu\text{m}$  sand, III and 550- $\mu\text{m}$  sand, and IV and 400- $\mu\text{m}$  sand. All other sand and gravel treatments exhibited little to no enhancement. Data from sediment bed experiments are listed in Tables 4 and 5.

Table 4. Data from sand bed deposition experiments. Bold values indicate average measurement applied for this experiment.

Flume	$d_g$ ( $\mu\text{m}$ )	$u_*$ ( $\text{cm s}^{-1}$ )	Suspension	$w_s$ ( $\text{cm s}^{-1}$ )	$w_d$ ( $\text{cm s}^{-1}$ )	$C_D$ ( $\times 10^4$ )	$m_c$ (mg)
17M	350	1.49	I	<b>0.0090</b>	0.0396	52	0.61
17M	350	1.15	I	0.0097	0.0355	60	0.54
17M	350	0.86	I	0.0084	0.0286	62	0.57
17M	350	0.29	I	<b>0.0090</b>	0.0043	68	0
17M	350	1.11	I	<b>0.0090</b>	0.0751	41	1.41
17M	350	0.98	I	<b>0.0090</b>	0.0478	45	1.13
17M	350	1.00	I	<b>0.0090</b>	0.0250	53	0.99
17M	350	0.62	I	<b>0.0090</b>	0.0126	54	1.64
17M	350	0.74	I	<b>0.0090</b>	0.0374	42	2.11
17M	350	0.53	I	<b>0.0090</b>	0.0097	64	1.67
17M	350	0.34	I	<b>0.0090</b>	0.0069	60	1.44
17M	350	0.60	I	<b>0.0090</b>	0.0230	55	1.06
17M	350	0.50	I	<b>0.0090</b>	0.0146	62	1.63
17M	350	0.62	II	<b>0.0054</b>	0.0020	52	1.90
17M	350	0.43	II	<b>0.0054</b>	0.0016	65	0.54
17M	350	0.76	II	<b>0.0054</b>	0.0017	60	0.83
17M	350	0.94	II	<b>0.0054</b>	0.0029	62	0.72
RTF	550	0.62	II	0.0068	0.0069	37	0.18
RTF	550	0.94	II	0.0068	0.0085	39	0.58
RTF	550	0.34	II	0.0067	0.0045	48	0.20
RTF	550	1.05	II	0.0066	0.0134	33	0.15
RTF	550	0.47	II	0.0068	0.0107	45	0.21
RTF	550	0.23	II	0.0059	0.0027	71	0.61
RTF	550	0.69	III	0.0227	0.0605	35	0.97
RTF	550	0.28	III	0.0353	0.0480	54	0.19
RTF	550	0.42	III	0.0370	0.0975	45	1.08
RTF	550	0.91	III	0.0500	0.1415	34	0.72
RTF	550	0.51	III	0.0447	0.1380	36	1.28
RTF	550	0.72	III	0.0360	0.1580	38	0.44
RTF	400	0.69	IV	0.0036	0.0210	24	1.00
RTF	400	0.34	IV	0.0038	0.0050	22	0.54
RTF	400	0.80	IV	0.0036	0.0180	24	0.40
RTF	400	0.50	IV	0.0048	0.0060	24	0.38

*Sediment core analysis*—Results from sediment cores confirmed the deposition amounts calculated from water samples for sand bed experiments (Fig. 6b). The points farthest from the 1:1 curve (in box on right side of plot) are results from the first three runs conducted. These experiments were subject to large errors in  $m_c$  because of the inclusion in the filter weights of plastic dishes that were not checked for consistent weights through drying. This error source was eliminated in all later experiments. For some experiments, the measured mass in the core was below the detection limit for this method (0.3 mg). Deviations from the 1:1 curve below this limit are not telling of any discrepancy in the two methods.

The sectioned cores revealed elevated concentrations of fine particles deeper in the sediment bed relative to the still-water experiments (Fig. 7a). Profiles taken at 1 and 3 h under still water show little change in time (Fig. 7b). The profile center of mass shifts down 1 mm over the 2-hr interval, corresponding to a settling velocity of  $1.5 \times 10^{-5} \text{ cm s}^{-1}$  (or  $<1\%$  of the particle settling velocity). Both of these observations support the idea that particles are entering the bed and penetrating into the sediment via fluid forcing driven by the flow, not settling within the sediment bed.

Table 5. Data from coarser sediment bed deposition experiments.

Flume	$d_g$ (cm)	$u_*$ ( $\text{cm s}^{-1}$ )	Suspension	$w_s$ ( $\text{cm s}^{-1}$ )	$w_d$ ( $\text{cm s}^{-1}$ )	$C_D$ ( $\times 10^4$ )
17M	1.23	0.34	II	0.0046	0.0011	54
17M	1.23	1.48	II	0.0070	0.0192	66
17M	1.23	2.67	II	0.0044	0.0255	67
RTF	1.23	0.84	II	0.0065	0.0165	53
RTF	1.23	1.29	II	0.0066	0.0162	55
RTF	1.23	2.43	II	0.0067	0.0148	55
RTF	1.23	0.87	II	0.0067	0.0095	53
RTF	1.23	0.38	II	0.0067	0.0016	51
RTF	1.23	0.21	II	0.0067	0.0009	49
RTF	1.23	0.58	II	0.0068	0.0136	51
RTF	1.23	3.36	II	0.0068	0.0049	58
RTF	1.23	0.40	II	0.0067	0.0033	35
RTF	1.23	4.08	II	0.0069	0.0136	57
RTF	1.23	0.20	II	0.0067	0.0091	40
RTF	1.23	0.76	III	0.0249	0.0120	45
RTF	1.23	2.23	III	0.0166	0.0492	51
RTF	1.23	4.19	III	0.0467	0.1060	57
RTF	0.13	0.82	II	0.0064	0.0100	34
RTF	0.13	0.43	II	0.0064	0.0050	33
RTF	0.13	1.25	II	0.0064	0.0120	32

## Discussion

*Comparison of results to previous deposition research*—This study provides a first look at the distinctions between two steps in fine-particle deposition: delivery and retention. The results of this work demonstrate that particle delivery needs to be coupled with effective particle retention in order to enhance deposition. The increase of deposition enhancement with grain Reynolds number supports the idea that increased turbulence at the interface supplies additional particles to the bed. The distinctions between deposition results for suspensions II and III to the 550- $\mu\text{m}$  sand bed and for suspensions I and II to the 350- $\mu\text{m}$  sand bed reveal the importance of interactions between particles and grains in the retention of delivered particles. These hypotheses are supported by previous investigations into the dynamics of particle deposition.

A common theme in studies of the alteration of deposition rates to sediment beds is the increase of particle delivery because of bed roughness. The model derived by Dade et al. (1991) predicts large enhancements of fine-particle deposition to sediment beds at high grain Reynolds numbers. The observations for high  $R_*$  reported in this study and by Einstein (1968) do not follow the model predictions (Fig. 8). The Dade model focuses on stable flow structures near a roughness capable of mediating the particle flux to a boundary that is a perfect sink. The discrepancy between model and observations reveals the need to mediate deposition predictions with a retention mechanism as well.

Previous investigators have observed the control of deposition rate by processes within granular beds. Hoyal et al. (1997) demonstrated the potential for filtration of particles from the flow by sand grains on the boundary. However, the experiments were conducted in a stir chamber, making com-

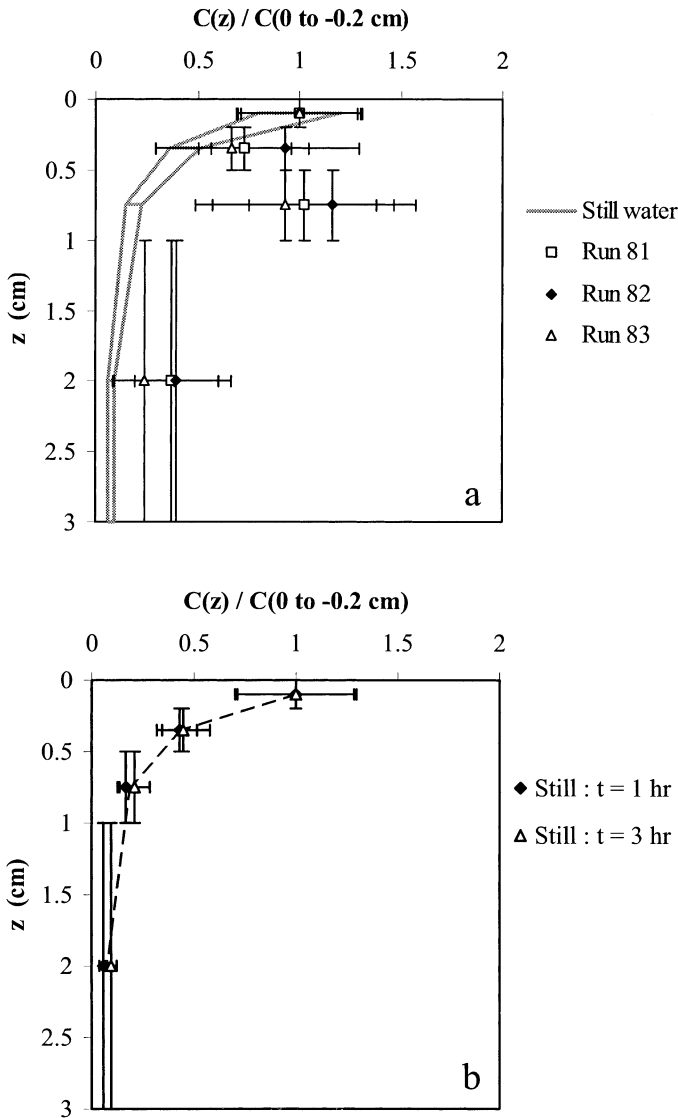


Fig. 7. Results from sectioned cores for 400- $\mu\text{m}$  sand experiments. (a) Flume experiment profiles. Still-water data contained in gray outline with horizontal bars at data locations. (b) Still-water results for different sampling times. Mean profile plotted as solid line. In both plots, vertical bars denote depth interval for measurement and horizontal error bars represent  $\pm 1$  SD. All particle concentrations in profile normalized by the interface value (0 to  $-0.2$  cm).

parison between their data and that of an open-channel boundary layer flow impossible. Flume measurements of fluid and particle penetration several grain diameters into flat sediment beds by Huettel et al. (1996) suggests that a fluid flux into the bed exists and is capable of increasing deposition rates relative to gravitational settling. If the near bed flows penetrate into the bed and filtration occurs, then deposition is enhanced.

*Check for aggregation in flume*—The rapid removal of fine particles from the water column is usually assumed to be due to aggregation. Two sets of experiments were undertaken to ensure that aggregation played no role in the en-

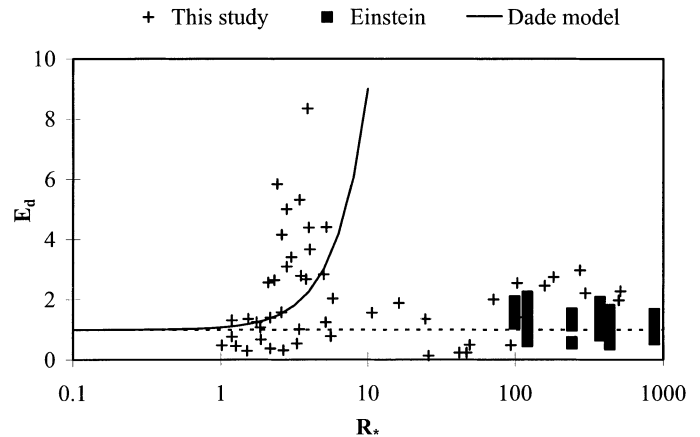


Fig. 8. Comparison of Dade model predictions and deposition results for all experiments and from Einstein (1968). Horizontal line represents no enhancement of deposition ( $E_d = 1$ ).

hancement observed in this study. Flume experiments over smooth panels were repeated with both freshwater and seawater suspensions. Three flume experiments with similar flow conditions were executed for each water type. Both the freshwater ( $u_* = 0.56 \pm 0.03 \text{ cm s}^{-1}$ ) and seawater ( $u_* = 0.55 \pm 0.01 \text{ cm s}^{-1}$ ) runs resulted in similar  $w_d$  values ( $0.017 \pm 0.002$  and  $0.014 \pm 0.003 \text{ cm s}^{-1}$ , respectively) and nearly identical time series measurements (Fig. 9).

*Link between deposition and drag coefficient*—Recent studies have highlighted the ability of permeable sediment beds to allow fluid intrusion near topography (e.g., Thibodeaux and Boyle 1987; Huettel et al. 1996). These studies include observations of the delivery of particles in pressure-driven, interfacial flows and some discussion of the potential for sedimentary control of the net deposition rate. A common theme is that the increases in deposition are associated with increases in the drag exerted on the fluid by the bed.

Flat sediment beds should not exhibit this correlation between drag and deposition. The drag coefficients for flat-bed experiments were obtained by integrating the best fit mean velocity profile to obtain  $U$ . Drag coefficients and deposition

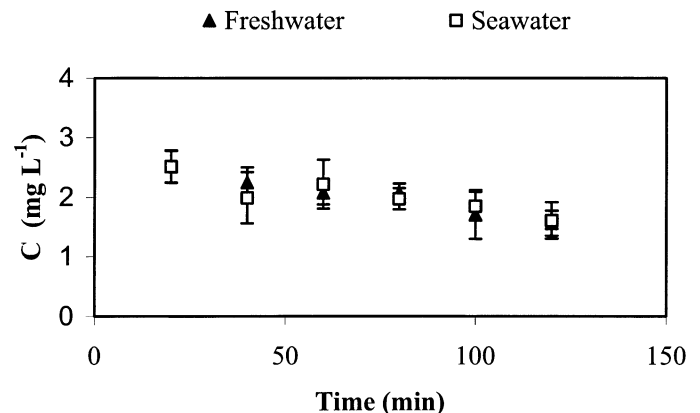


Fig. 9. Aggregation test results. Time series of concentration in freshwater and seawater. Error bars represent  $\pm 1$  SD.

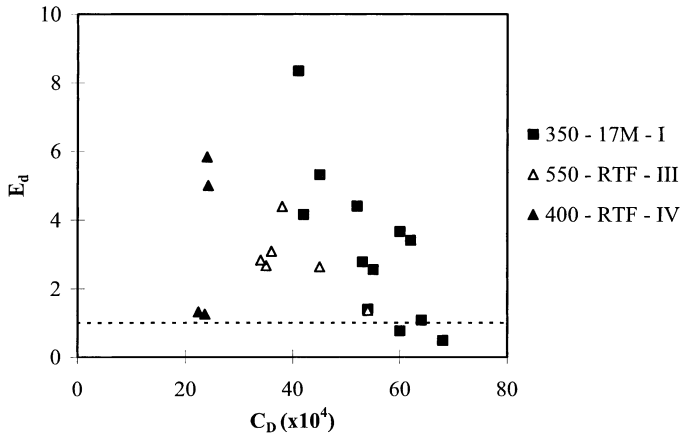


Fig. 10. Drag coefficient relative to deposition results for all experiments with significant enhancement. Symbols are the same as in Fig. 5.

velocities for the three treatments with significant enhancement were compared (Fig. 10). In none of these cases was the correlation positive. In fact, the correlations were negative for the treatments with significant variation in  $C_D$  (all but 400- $\mu\text{m}$  sand). This evidence dismisses the possibility that topography is responsible for the observed deposition enhancement.

The negative correlation between drag and deposition could simply be due to the nature of the boundary layer over the sediment. The general expression for drag coefficient for turbulent boundary layers in open channels is shown in Eq. 29.

$$C_D = \kappa^2 \left\{ \ln \left( \frac{h}{d_g} \right) + [\kappa B(R_*) + \Pi - 1] \right\}^{-2} \quad (29)$$

For smooth turbulent flows, the value of  $B$  increases with  $R_*$ , leading to a decrease in drag coefficient with grain Reynolds number. Coupled with the positive correlation between  $E_d$  and  $R_*$ , the reduced drag coefficient for large enhancement would be expected. However, the variability in drag coefficient is too large to be attributable only to the increase in  $B$ . Another mechanism, one that reduces drag while increasing interfacial flux, might be contributing to the observed enhancements.

One possibility is the induction of slip at the sediment–water interface. Reductions in drag because of flow within a permeable boundary have been observed by other investigators (e.g., Beavers and Joseph 1967; Richardson and Parr 1991). By adding a slip velocity ( $u_s$ ) to the velocity profile, the drag coefficient becomes

$$C_D = \kappa^2 \left[ \ln(R_h) + (5.5\kappa + \Pi - 1) + \kappa \frac{u_s}{u_*} \right]^{-2} \quad (30)$$

The existence of subsurface flow and slip at the interface could be indicated by changes in the drag coefficient based on measurements taken above the sediment–water interface. Although the existence of slip could explain the observed relationship between drag and deposition, the mechanism that drives this flow is not apparent. The most promising lead is a diffusive flux of fluid and momentum across the

Table 6. Enhancement ranges depending on the sediment particle treatment.

$d_g$ ( $\mu\text{m}$ )	$d_p$ ( $\mu\text{m}$ )	$D_R$	Range of $E_d$
350	12	29	0.5–8.3
400	13	31	1.3–5.8
350	8	44	0.5–0.8
550	25	22	1.4–4.4
550	8	69	0.5–2.0

sediment–water interface. Direct measurements of flow profiles within porous boundaries (Ruff and Gelhar 1972; Nagoka and Ohgaki 1990) confirm that interstitial velocity might be driven by a downward diffusion of momentum. Richardson and Parr (1988) used interfacial diffusion to describe the effusion of solutes from sediments subjected to runoff flow. This scenario can be inverted to describe the transport of particles into the sediment bed. Their work demonstrated a positive correlation between flux and shear velocity for each sediment tested. This is consistent with the observed increase in  $w_d$  with  $R_*$  for most treatments in this study.

*Filtration at the sediment–water interface*—Although the dependence of deposition on flow is clear in Fig. 6a, there are different levels of enhancement for different particle and sediment treatments under similar flow conditions. This suggests that the grain diameter ratio is also important in predicting the amount of enhancement. This dependence is demonstrated in Table 6, where, within the two groups of sand treatments, different ranges in  $E_d$  were measured depending on  $D_R$ . The tendency to have larger enhancements for smaller bed grain ratios is consistent with the idea that filtration is more efficient for larger particles within the same sediment matrix.

The filtration mechanism expected for  $D_R$  values between 10 and 30 is called straining (McDowell-Boyer et al. 1986). This mechanism involves the capture of particles in the narrow passages of the granular pore space. The filtration efficiency for straining rapidly declines as  $D_R$  increases. The possibility exists that particles “hiding” behind bed grains at the interface contribute to particle retention. Both hiding and straining depend on the relative cross sectional areas of particles and grains and, therefore, have a similar dependency on  $D_R$ . Without measurements directed at revealing the distinction between these retention modes, both mechanisms combined are considered to be bed filtration. The dependence of enhancement on the bed grain ratio suggests that, in addition to particle delivery via interfacial diffusion, particle retention in the bed by filtration is critical to deposition enhancement.

*Enhancement of deposition beyond flat beds*—It is important to recognize how these processes interact in the environments modeled within these experiments. The delivery of particles via interfacial diffusion is the “supply” of particles to the sediment. Flume observations support the idea that more energetic flows or more permeable beds lead to an

increase in delivery. However, this increase does not necessarily translate into an enhancement of deposition. The filtration efficiency of the sediment is the “demand” for particles. Without efficient filtration, a large particle supply does not translate to a large enhancement, as observed here and by Einstein (1968). The coupling of “supply and demand” is necessary for the enhancement of deposition.

Observations of enhanced deposition to flat sediment beds lead to the conclusion that both delivery and retention of particles are being driven by processes at the grain scale. If this is the case, then it is likely that these mechanisms could be acting in environments more complicated than a flat sediment bed (i.e., rippled beds). Several complications, including separating flows and sediment transport, can disrupt either step and limit the importance of the processes observed in this study. Future work comparing these results with similar measurements in more complicated environments will reveal the applicability of these results beyond flat beds.

This study presents observations of fine-particle deposition to permeable sediment beds. Enhanced rates for specific treatments of flow, suspension, and bed grain size were measured. Control experiments over impermeable beds resulted in no enhancement relative to settling. For coarser sediment beds, deposition rates were not enhanced, consistent with the results reported by Einstein (1968). Other potential explanations for the enhancement, such as aggregation or topography, were not responsible for the observed rates. In fact, the inspection of variations in deposition with the drag coefficient revealed that the mechanism that enhances particle delivery to the bed also reduces the drag in the channel. Additional evidence of a new set of mechanisms controlling deposition is the dependence on the grain diameter ratio, implicating filtration of particles within the sediment bed as critical to enhancement of deposition. These results inspire the pursuit of a conceptual model capable of predicting conditions for the enhancement of fine-particle deposition to permeable sediment beds.

## References

- AGRAWAL, Y. C., AND C. J. BELTING. 1988. Laser velocimetry for benthic sediment transport. *Deep-Sea Res.* **35**: 1047–1067.
- AL-KHAFI, A. W., AND O. B. ANDERSLAND. 1992. Geotechnical engineering and soil testing. Saunders College Publishing.
- BEAVERS, G. S., AND D. D. JOSEPH. 1967. Boundary conditions at a naturally permeable wall. *J. Fluid Mech.* **30**: 197–207.
- BOUDREAU, B. P. 1997. Diagenetic models and their implications. Springer-Verlag.
- BUTMAN, C. A., AND R. J. CHAPMAN. 1989. The 17-meter flume at the Coastal Research Laboratory. Part I: Description and user's manual. WHOI Tech. Rep. 89-10 (CRC Tech. Rep. 89-2).
- COLES, D. 1956. The law of the wake in the turbulent boundary layer. *J. Fluid Mech.* **1**: 191–226.
- DADE, W. B., A. R. M. NOWELL, AND P. A. JUMARS. 1991. Mass arrival mechanisms and clay deposition at the seafloor, p. 161–165. *In* R. H. Bennett, and others [eds.], *Microstructure of fine-grained sediments*. Springer-Verlag.
- EINSTEIN, A. 1906, reprinted 1956. On the theory of Brownian movement, p. 19–35. *In* R. Furth [ed.], *Investigations on the theory of Brownian movement*. Dover Publications.
- EINSTEIN, H. A. 1968. Deposition of suspended particles in a gravel bed. *J. Hydraul. Div., ASCE* **94**: 1197–1205.
- FRIES, J. S. 2002. Enhancement of fine particle deposition to permeable sediments. Ph.D. thesis. MIT/WHOI, 2002-02.
- GRASS, A. J. 1971. Structural features of turbulent flow over smooth and rough boundaries. *J. Fluid Mech. (part 2)* **50**: 233–255.
- HOYAL, D.C.J.D., M. I. BURSIK, J. F. ATKINSON, AND J. V. DEPINTO. 1997. Filtration enhances suspended sediment deposition from surface water to granular permeable beds. *Water Air Soil Pollut.* **99**: 157–171.
- HUETTEL, M., W. ZIEBIS, AND S. FORSTER. 1996. Flow-induced uptake of particulate matter in permeable sediments. *Limnol. Oceanogr.* **41**: 309–322.
- KOZENY, J. 1927. Über kapillare Leitung des Wassers im Boden. *Sitzungsber. Akad. Wiss. Wien* **136**: 271–306.
- MCDOWELL-BOYER, L. M., J. R. HUNT, AND N. SITAR. 1986. Particle transport through porous media. *Water Resour. Res.* **22**: 1901–1921.
- NAGOKA, H., AND S. OHGAKI. 1990. Mass transfer mechanism in a porous riverbed. *Water Res.* **24**: 417–425.
- NEZU, I., AND W. RODI. 1986. Open-channel flow measurements with a laser doppler anemometer. *J. Hydr. Eng., ASCE* **112**: 335–355.
- NINO, Y., AND M. H. GARCIA. 1996. Experiments on particle-turbulence interactions in the near-wall region of an open channel flow: Implications for sediment transport. *J. Fluid Mech.* **326**: 285–319.
- NITTROUER, C. A., AND L. D. WRIGHT. 1994. Transport of particles across continental shelves. *Rev. Geophys.* **32**: 85–113.
- NOWELL, A. R. M., P. A. JUMARS, R. F. L. SELF, AND J. B. SOUTHWORTH. 1981. The effects of sediment transport and deposition on infauna: Results obtained in a specially designed flume, p. 247–268. *In* G. Lopez, G. Taghon, and J. Levinton [eds.], *Ecology of marine deposit feeders*. Springer-Verlag.
- PACKMAN, A. I., AND N. H. BROOKS. 2001. Hyporheic exchange of solutes and colloids with moving bed forms. *Water Resour. Res.* **37**: 2591–2605.
- RICHARDSON, C. P., AND A. D. PARR. 1988. Modified fickian model for solute uptake by runoff. *J. Environ. Eng.* **114**: 792–809.
- , AND ———. 1991. Friction and free-surface flow over porous media. *J. Hydraul. Eng., ASCE* **117**: 1496–1512.
- RUFF, J. E., AND L. W. GELHAR. 1972. Turbulent shear flow in porous boundary. *J. Eng. Mech. Div., ASCE* **98**(EM4): 975–991.
- SCHLICHTING, H. 1968. *Boundary-layer theory*, 6th ed. McGraw-Hill.
- THIBODEAUX, L. J., AND J. D. BOYLE. 1987. Bedform-generated convective transport in bottom sediment. *Nature* **325**: 341–343.
- TROWBRIDGE, J. H., W. R. GEYER, C. A. BUTMAN, AND R. J. CHAPMAN. 1989. The 17-meter flume at the Coastal Research Laboratory. Part II: Flow characteristics. WHOI Tech. Rep. 89-11 (CRC Tech. Rep. 89-3).
- WARD, J. C. 1964. Turbulent flow in porous media. *J. Hydraul. Div., ASCE* **90**(HY5): 1–12.
- WHEATCROFT, R. A., J. C. BORGELD, R. S. BORN, D. E. DRAKE, E. L. LEITHOLD, C. A. NITTROUER, AND C. K. SOMMERFIELD. 1996. The anatomy of an ocean flood deposit. *Oceanography* **9**: 158–162.

Received: 19 April 2002  
Accepted: 2 October 2002  
Amended: 28 October 2002